Astronomical and Astrophysical Transactions (*AApTr*), 2025, Vol. 35, Issue 1, pp. 83–106,
ISSN 1055-6796, Photocopying permitted by license only, ©Cambridge Scientific Publishers

Rotation measure as a tracer of disk outflows

M.A. Buldakov*, A.S. Andrianov

Astro Space Center, Lebedev Physical Institute, 84/32 Profsoyuznaya St., 117997 Moscow, Russia

Received 8 August, 2024; accepted 5 December, 2024

The aim of this paper is to consider possible interrelations between characteristics of turbulence in accretion disks, such as α-parameters, mass loss rate due to vertical wind driven by magneto-rotational instability (MRI) and the Faraday rotation measure (RM). We study numerically temporal variations of rotation measure for the line of sight perpendicular to the disk plane, turbulent α-parameter, Reynolds and Maxwell stresses, and the gas mass outflow rate through vertical boundaries. We find that although the magnitude of variations is rather high, all these variables grossly show correlated behaviour. Numerical simulations are approached in a shearing box model. Standard assumptions are accepted for the initial state of the gas in disk: isothermal disk with vertical hydrostatic equilibrium, uniform density distribution in the plane and vanishing magnetic flux through vertical boundaries. We analyze evolution and statistical characteristics of RM, α-parameter and vertical mass outflow. We found pairwise correlations between these quantities. Such correlations are predicted by model of Shakura–Sunyaev accretion disk with zero net vertical magnetic flux. Correlations between RM and vertical mass outflow in principle can be measured in future observations of Sgr A* by ngEHT, so consistency of considered model with real astrophysical disks can be tested in the near future. It is also found that the period of oscillations of RM, α-parameter and vertical mass outflow is approximately equal to the period of dynamo cycle. Measurements of RM can provide information about evolution of α-parameter and vertical mass outflow. Correlations found between RM, turbulence α-parameter and mass flux through vertical boundaries can be used for diagnostics of physical state of the accretion flow mimicked by the shearing box model. Possible implications for astrophysical disks are discussed.

Keywords: Accretion disks, magnetohydrodynamics, numerical simulation

1 Introduction

Magnetohydrodynamic turbulence is thought to be the main driver of mass transfer in accretion disks (Shakura and Sunyaev 1973; Lynden-Bell and Pringle 1974; Balbus and Hawley 1998). S.A. Balbus and J.F. Hawley (Balbus and Hawley 1991; Hawley

*Email: buldakov@phystech.edu

and Balbus 1991) concluded that the most powerful mechanism to initiate turbulence in accretion disks is the magnetorotational instability (MRI) first described by E.P. Velikhov (Velikhov 1959) and S. Chandrasekhar (Chandrasekhar 1960). MRI develops in shearing flows under arbitrary weak magnetic field, and as such can be applicable in a wide class of astrophysical disks and flows with the velocity shear. Later on T.K. Suzuki and S.-I. Inutsuka (Suzuki and Inutsuka 2009) and Suzuki et al. 2010 proposed that MRI might be responsible not only for the radial mass transport in accretion disks, but for the vertical disk outflows as well. Since then several attempts have been undertaken to study MRI-driven disk winds (see discussions in (Bai and Stone 2013; Fromang et al. 2013)).

It is of interest to investigate whether the characteristics of disk structures that are studied by numerical models can be connected with observational characteristics of the disk and measured in observational experiments. The studies of local (shearing box) and global disk simulations show that the turbulent and outflow structures can affect time evolution of magnetic fields, e.g. dynamo-effect is a typical phenomenon observed in accretion disk simulations (Brandenburg et al. 1995; Shi et al. 2010). Time evolution of magnetic fields can be studied by measurements of rotation measure (RM), which is an important observational characteristic of the disk (Sharma et al. 2007; Kuo et al. 2014; Li et al. 2016). This paper aims to investigate possible relations between the characteristics of turbulence such as α-parameter, characteristics of gas outflow and the observational characteristics of the disk (namely, RM). We can study this question by investigating correlational properties of these quantities. High correlations between some disk parameter and RM would indicate that one can get information about evolution of that characteristic by measurements of RM. We study the question whether one can find correlations between RM, α-parameter and the vertical mass outflow in shearing box simulations of accretion disks.

We use local shearing box model because for a detailed study of the turbulent processes in the disk, it is necessary to simulate processes occuring on small spatial scales (Latter et al. 2010). Such scales can only be studied in local models with sufficiently high resolution (Hawley et al. 2013). In (Hawley et al. 2013) it is shown that the minimum required grid resolution to resolve the most unstable MRI mode is ≈ 32 points per characteristic height of the disk. Such resolutions can only be achieved in local models. Currently, it is not possible to simulate the global accretion disk with such resolution.

2 Model

2.1 Numerical setup

The calculations are carried out by using the shearing box model in which local Cartesian frame of reference corotating with the Keplerian accretion disk with a frequency Ω at a large radius R_0 is considered (Hawley et al. 1995). It is assumed that the plasma in the computational domain is described by standard ideal MHD equations (Stone et al. 1996). Vertical gravitational force is added to ideal MHD equations and it leads to vertical density stratification. MHD equations are solved on the 3D uniform rectangular grid by means of PLUTO code (Mignone et al. 2007). We study

models with isothermal equation of state $P = \rho c_s^2$. The described code configuration is similar to one used in Bodo et al. 2014.

The magnetic Prandtl number P_m is not explicitly assigned in case of ideal MHD simulations and it depends on numerical dissipation scales. Both dissipation scales are roughly equal to the grid scale, so $P_m \sim 1$ in our calculations. P_m of the order of unity in ideal MHD simulations of accretion disks are reported in e.g. Minoshima et al. 2015; Lesur and Longaretti 2007; Brandenburg 2014; Held et al. 2024.

We use magnetic field configuration with zero net vertical magnetic flux. The initial magnetic field component B_z is defined as

$$B_z(0) = B_{z0} \cdot \sin(\frac{2\pi}{L_x}x), \tag{1}$$

where L_x is the computational domain size in x direction. The coefficient B_{z0} is chosen so that the initial plasma parameter $\beta_0 = 8\pi P_0/B^2$ (the ratio of gas pressure to magnetic pressure) is equal to 10^3. The initial configuration of the disk is in the hydrostatic equilibrium. The initial density profile is $\rho(0) = \exp(-z^2/H^2)$, where H is a characteristic scale height of the disk. Code units are chosen so that $H = \sqrt{2}c_s/\Omega$, where c_s is a speed of sound and Ω is an angular rotation frequency of the disk, and $c_s = 1$, $\Omega = 1$ in code units. Initial pressure in the midplane of the disk $P_0 = 1$. In order to initiate MRI instability and development of turbulence, velocity fluctuations were added for the velocity component v_y with an amplitude about $10^{-3} \cdot v_y$. The size of the computational domain is $-0.5H < x < 0.5H$, $0 < y < \pi H$, $-4H < z < 4H$. The duration of calculations is $160 \cdot T$, where T is a period of disk rotation.

The boundary conditions are shear-periodic in x direction and periodic in y direction. Modified outflow boundary conditions are applied in z direction and are formulated as follows. Magnetic fields are copied in the ghost zones with zero gradient condition. Densities in the ghost zones are extrapolated assuming hydrostatic equilibrium and constant temperature $T_{eq} = 0.5 \cdot \Omega^2$ in the ghost zones. Velocities are copied in the ghost zones with zero gradient condition and also additional condition for the velocity component v_z is applied: if there is a mass inflow in the ghost zone cells ($v_z > 0$ at the lower boundary or $v_z < 0$ at the upper boundary), v_z velocity in those cells is set to zero, so there is no mass inflow in the computational domain.

We carry out four calculations with different grid resolutions. Model SB1 has resolution 32×96×256 grid points on x, y, z axes correspondingly, i.e. 32 points per scale height. A model SB2 with double resolution 64×192×512 (64 points per scale height) is also analyzed. For each of these two models additional calculations with double resolution on z axes are performed: models SB1-Z and SB2-Z with resolutions 32×96×512 and 64×192×1024, correspondingly. Our fiducial model is model SB2 with higher resolution and aspect ratio of a grid cell 1:1:1. The main characteristics of models are summarized in Table 1.

Table 1 Summary of the main characteristics of models.

Model	Resolution	Calculation grid size	β_0	Calculation time, T
SB1	32×96×256	1H×3H×8H	10^3	160
SB2	64×192×512	1H×3H×8H	10^3	160
SB1-Z	32×96×512	1H×3H×8H	10^3	160
SB2-Z	64×192×1024	1H×3H×8H	10^3	160

2.2 Main quantities

We use the following notations for the averages of quantities. For a given quantity F we define:

$$\langle F\rangle = \frac{\int_V F dV}{V} \tag{2}$$

the volume average,

$$\overline{F} = \frac{\int_{x,y} F dx dy}{\int_{x,y} dx dy} \tag{3}$$

the horizontal average and

$$\tilde{F} = \frac{\int_T^{T+\Delta T} F dt}{\Delta T} \tag{4}$$

the time average, where V is the volume of computational domain and time averaging is performed over the time interval $(T,\, T+\Delta T)$.

Here we consider the main quantities analysed in simulations. Turbulence α-parameter of N.I. Shakura and R.A. Sunyaev (Shakura and Sunyaev 1973) is commonly used for characterizing the radial angular momentum transport rate in the disk (Hawley et al. 1995; Bai and Stone 2013; Brandenburg et al. 1995). Turbulence α-parameter is calculated as the averaged component of stress tensor (Maxwell or Reynolds stress or sum of both of them) normalized to the averaged gas pressure. Maxwell and Reynolds stresses are defined as $T_M = -\left(B_x \cdot B_y\right)/4\pi$ and $T_R = \rho \upsilon_x \delta\upsilon_y$, correspondingly, where B is the magnetic field, υ is the gas velocity, $\delta\upsilon_y = \upsilon_y + (3/2)\,\Omega x$. The definitions of α parameters are

$$\alpha_M = \frac{\int \overline{T}_M(z)\, dz}{\int \overline{\rho}(z)\, {c_s}^2 dz} \tag{5}$$

for α-parameter corresponding to Maxwell stress,

$$\alpha_M = \frac{\int \overline{T}_R(z)\, dz}{\int \overline{\rho}(z)\, {c_s}^2 dz} \tag{6}$$

for α-parameter corresponding to Reynolds stress and

$$\alpha = \frac{\int \left(\overline{T}_M(z) + \overline{T}_R(z)\right) dz}{\int \overline{\rho}(z)\, {c_s}^2 dz} \tag{7}$$

for the total α-parameter. In our calculations $\alpha_R(t) \approx 0.25 \cdot \alpha_M(t)$ and the ratio of α_R to α_M is approximately the same for all four models. This ratio is typical for

accretion disk simulations (Jiang et al. 2013; Hawley et al. 1995; Sano et al. 2004; Davis et al. 2010).

We also study total mass flux through vertical boundaries F_{bound}. We define F_{bound} as

$$F_{bound} = |\int_{x_l,y_l} \rho v_z| + \int_{x_u,y_u} \rho v_z \tag{8}$$

where x_l, y_l denote grid points of the horizontal plane at the lower vertical boundary and x_u, y_u denote grid points of the horizontal plane at the upper vertical boundary.

We assume that the disk is viewed face-on with line of sight perpendicular to the disk plane and in this case we calculate RM (in arbitrary units) as

$$RM = \int_z B_z \cdot \rho dz \tag{9}$$

for a given point (x, y) in the horizontal plane of the computational grid. We calculate local RM for every of (x, y) grid points and then take average of it, thus obtaining horizontally averaged RM ($\overline{RM}$).

3 Results

Our aim is to analyze correlations between rotation measure (RM) and characteristics of turbulence and mass outflow obtained in modeling. We begin this section with description of the main characteristics of models, such as turbulence α-parameter and mass outflow through vertical boundaries. The next part of this section describes techniques that we use to calculate correlational properties of characteristics of the disk and the final part contains our main results of the correlation analysis.

3.1 Properties of turbulence and mass outflow

Time evolution of α_M for our four models is shown in Figure 1. We measure time in periods of disk rotation (orbits) and the unit of time is $2\pi/\Omega$.

In the rest of the paper we provide detailed description of the results only for the fiducial model SB2. From the start of the computation growing magnetorotational instability (MRI) leads to the development of turbulence. Starting from $t \approx 10$ orbits turbulence reaches non-linear stage. Then until the end of computation the disk is fully turbulent and α_M is mainly oscillating around its mean value $\tilde{\alpha_M} \approx 0.015$ with some large peaks of turbulent activity, e.g. at $t = 20$ and $t = 105$ orbits. There is also a notable feature in time evolution of α_M for the model SB1-Z: especially large peak of turbulent activity can be seen at $t = 105$ orbits. The amplitude of this peak is twice as large as the typical amplitude of the other peaks. Such peak might be connected with irregularity of dynamo activity in the disk which is described below. It is worth noting that no dependence is found between time averaged α and grid resolution. In our calculations $\tilde{\alpha}$ is equal to 0.017, 0.018, 0.022, 0.017 for our models SB1, SB2, SB1-Z, SB2-Z, correspondingly. Higher value of $\tilde{\alpha}$ for the model SB1-Z is connected to the peak of turbulent activity at $t = 105$ orbits.

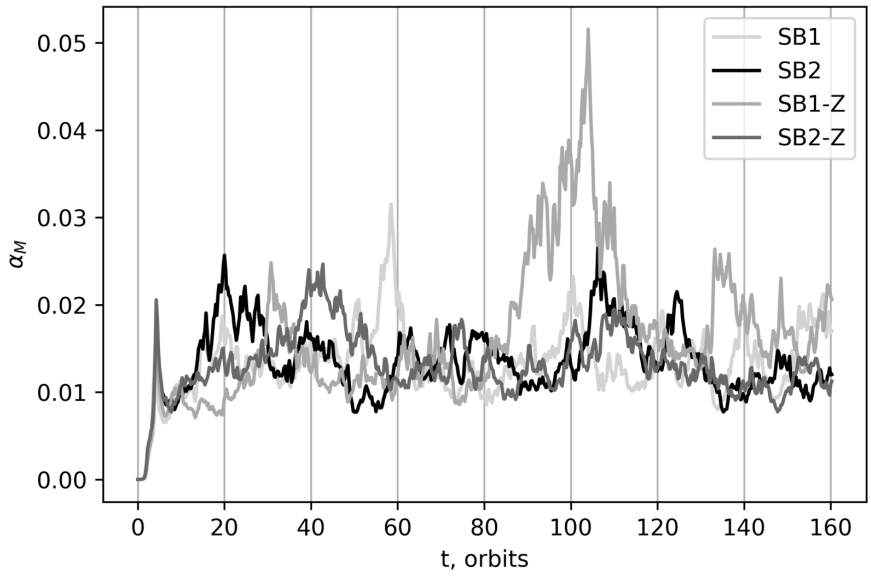


Figure 1 Time evolution of α_M for four models.

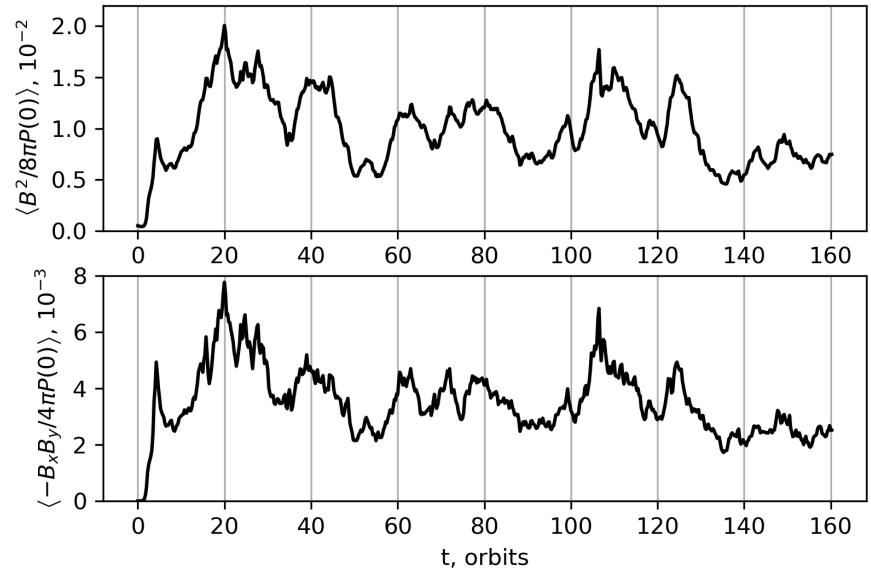


Figure 2 Time evolution of the volume averaged magnetic energy (top) and Maxwell stress (bottom) normalized to the pressure at the midplane of the disk $P(0)$ for the model SB2. Magnetic energy and Maxwell stress are measured in arbitrary units.

We also show time dependencies of magnetic energy and Maxwell stress in Figure 2 for the fiducial model SB2. Time evolution of these quantities is similar to time

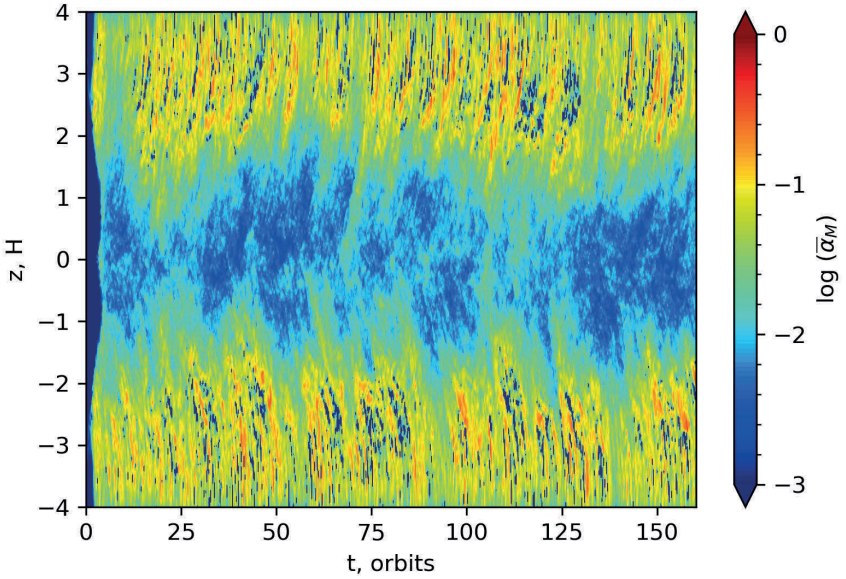


Figure 3 Time evolution of the horizontally averaged local $\alpha_M\,(z,t)$ for the model SB2.

evolution of α_M and they also show the evolution of MRI turbulence. After the initial rapid growth of MRI with a peak at $t \approx 4$ orbits magnetic energy and Maxwell stress fluctuate around their mean values. However, the initial peak of MRI growth is distinctly seen only in models SB2 and SB2-Z with higher resolution, but the initial peak is not so large in models SB1 and SB1-Z with lower resolution. According to the research of J.F. Hawley (Hawley et al. 2013), acceptable resolution for the description of MRI in shearing box calculations is achieved for $\gtrsim 32$ cells per scale height. All of our models satisfy this criterion, so our lower resolution models should be suitable for study of evolution of MRI turbulence.

Time evolution of the vertical structure of horizontally averaged local parameter α_M is shown in Figure 3. This local parameter $\overline{\alpha}_M$ is defined as

$$\overline{\alpha}_M\,(z,t) = \frac{\overline{T}_M\,(z,t)}{\overline{\rho}\,(z,t)\,{c_s}^2}\,. \tag{10}$$

It provides more detailed structure of α_M.

Local α-parameter $\overline{\alpha}_M\,(z,t)$ strongly varies with height: it is small near the mid-plane of the disk at $|z| \lesssim 2{\cdot}H$ and large near the top and bottom of the computational domain at $|z| \gtrsim 2 \cdot H$. This structure is similar to the results presented, e.g., in the work of Y. Io and T.K. Suzuki (Io and Suzuki 2014).

Mass outflow is an important characteristic of accretion disks. It is an inherent property of real astrophysical disks and we study the structure and time evolution of the outflow in our models. Due to our vertical boundary conditions we obtain a mass outflow which average efficiency is about 0.2 % of the initial mass of gas lost per orbit. Figure 4 shows time evolution of the total mass of gas M normalized on the initial mass of gas M_0 for four models with different grid resolutions.

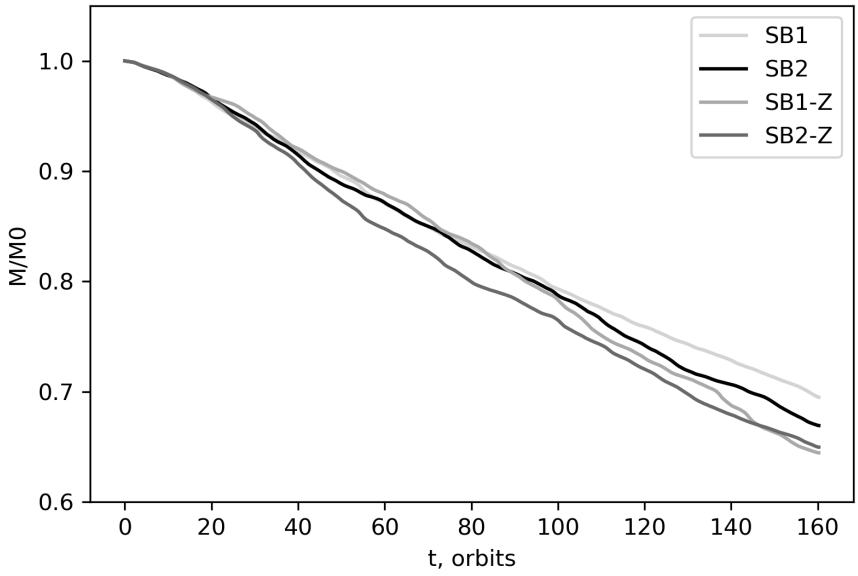


Figure 4 Time evolution of the total relative mass of gas M/M_0 for four models.

Mass outflow with approximately constant rate is seen for all four models. During the time course of calculations about 30% of the total mass of gas is lost through the

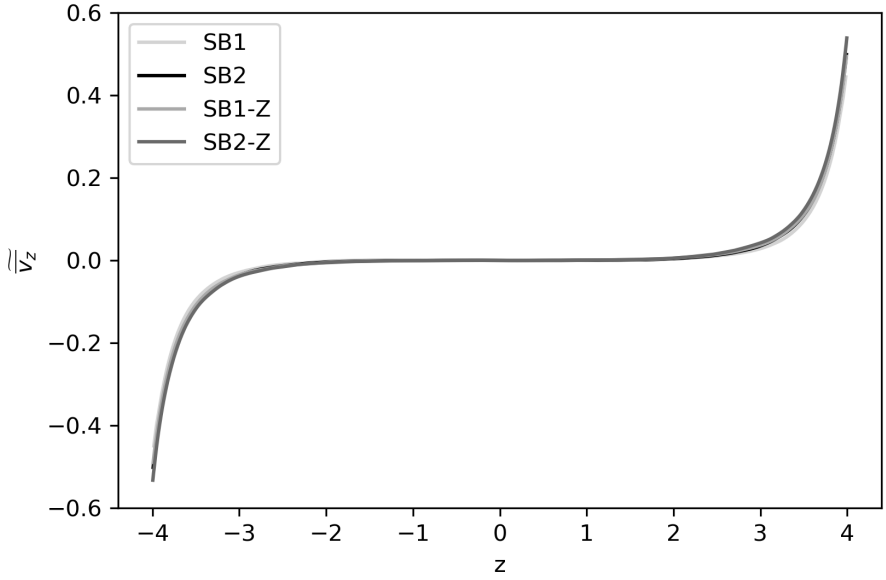


Figure 5 Vertical profile of horizontally and time averaged velocity v_z for four models. Time averaging is performed over the interval (20–140) orbits. Velocity is measured in arbitrary units.

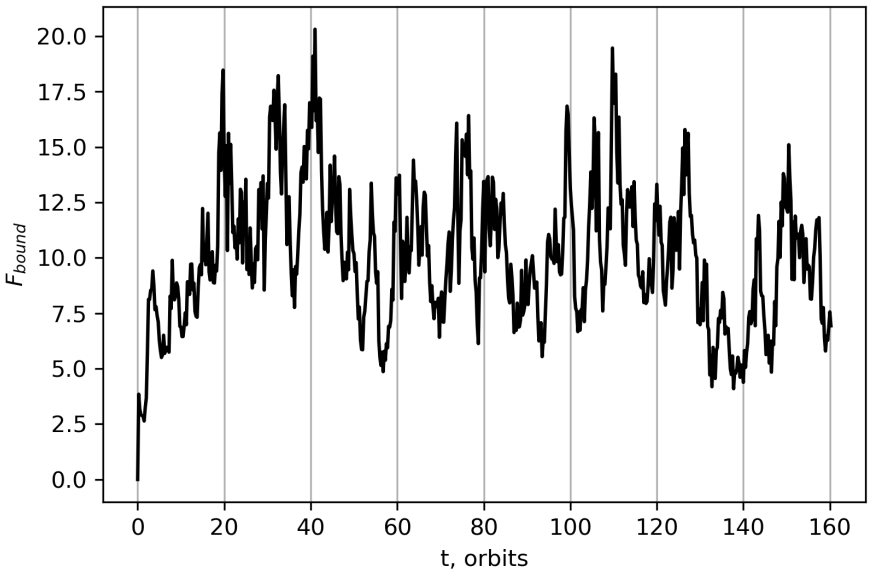


Figure 6 Time evolution of the total mass flux through vertical boundaries F_{bound} for the model SB2. Mass flux is measured in arbitrary units.

vertical boundaries of the computational domain. There is no systematic dependence of mass loss rate on grid resolution. Similar results were shown by Fromang et al. 2013 in their study of mass loss rate for the models with varying number of grid cells in the vertical direction. In this work shearing box models with net vertical magnetic field and plasma parameter $\beta = 10^4$ were considered. It is reported that 20% of the disk mass was lost from the computational box during 20 orbits, i.e. the mass outflow efficiency is about 1% of the initial mass of gas lost per orbit. The mass-loss rate per unit area in this model is in a good agreement with results reported in (Suzuki and Inutsuka 2009). In (Suzuki and Inutsuka 2009) it was also found that the mass outflow rate linearly increases with the magnetic pressure of the net vertical field. Our models have zero net magnetic flux and we expect the mass outflow efficiency < 1 %, so our value is in accordance with the expected value.

We show the vertical profile of horizontally and time averaged velocity v_z for four models in Figure 5. It rapidly increases near the vertical boundaries at $|z| > 3 \cdot H$.

The structure of the outflow can also be illustrated with time evolution of the total mass flux through vertical boundaries F_{bound}, which is shown in Figure 6 for the model SB2.

The mass flux has oscillating structure with some significant outbursts (e.g., at $t \approx 20$ and $t \approx 110$ orbits) that roughly correspond to the peaks seen in time evolution of α_M for SB2 calculation shown in Figure 1. It may indicate that those outbursts are connected with turbulent activity in the disk. The described properties of the outflow are in accordance with other papers (Fromang et al. 2013; Bai and Stone 2013; Moll 2012).

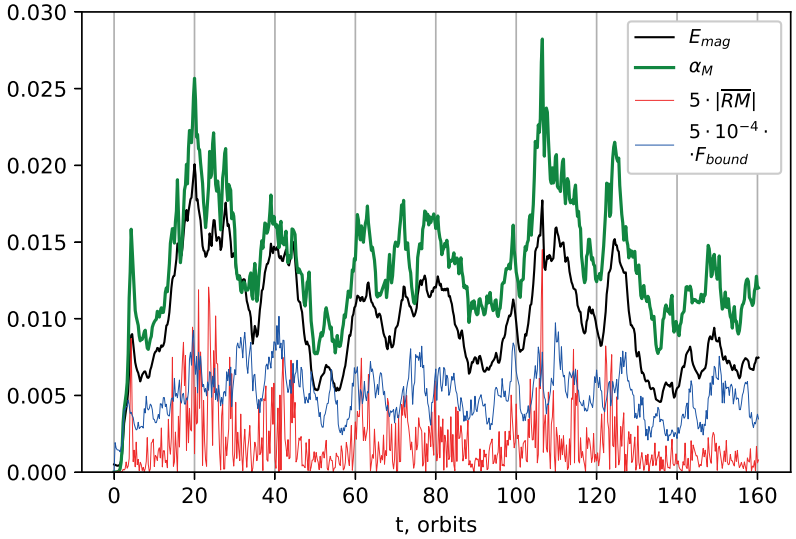


Figure 7 Time evolution of the volume averaged magnetic energy E_{mag} (black line), α_M (green line), $|\overline{RM}|$ (red line) and F_{bound} (blue line) for the model SB2. E_{mag}, $|\overline{RM}|$ and F_{bound} are measured in arbitrary units.

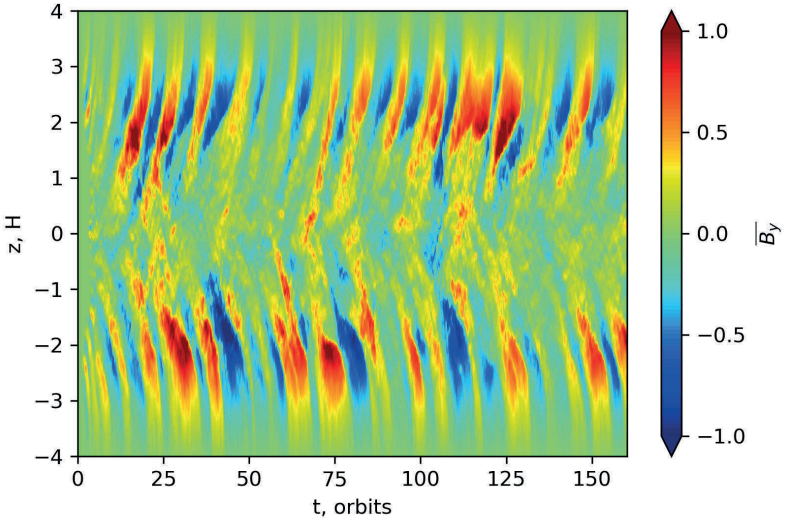


Figure 8 Contour plot of the horizontally averaged B_y for the model SB2. B_y is measured in arbitrary units.

For the purpose of additional illustration of quasi-oscillatory behaviour of such quantities as magnetic energy, rotation measure, α_M and F_{bound}, time evolution of these quantities are presented on a single figure in Figure 7. Several significant local maxima can be distinguished for all presented quantities, e.g. maxima at $t = 20, 28, 40, 53, 63, 72, 80, 99, 106, 125, 150$ orbits. It indicates that there is a

quasiperiodic behaviour of magnetic energy, $\overline{RM}$, α and F_{bound} with the periods about 10–20 orbits.

In Figure 8, we plot $\overline{B_y}$ over disk height and time for our fiducial model SB2. Evolution of the averaged azimuthal field $\overline{B_y}$ follows a typical butterfly diagram pattern with the period of oscillations ≈ 10 orbits. This is in agreement with other authors' results (Gressel and Pessah 2015; Dhang and Sharma 2019; Bai and Stone 2013; Flock et al. 2011). The effect of butterfly oscillations is suggested to be connected with the dynamo effect in accretion disks and magnetic buoyancy (e.g., it is described in Gressel 2010). The butterfly diagram has a similar structure for all our four models, but there are some differences for the models with higher and lower resolution. Dynamo cycles have good periodicity for the models with higher resolution SB2 and SB2-Z, while dynamo cycles for the low resolution models SB1 and SB1-Z show some irregularities in amplitudes and duration. For example, an especially long outburst with high amplitude can be seen in a butterfly diagram for the model SB1-Z (it is shown in Appendix A).

3.2 Study of correlational properties between turbulent and outflow characteristics of the disk and rotation measure

Here we describe the numerical techniques used for calculations of correlations between α, F_{bound} and RM.

We study time evolution of the horizontally averaged RM, i.e. $\overline{RM}\,(t)$, and study its properties and correlations with turbulent and outflow characteristics of modeled accretion disks (namely, with α_M and F_{bound}).

Time evolution of $\overline{RM}$ is shown in Figure 9. It has oscillating structure and changes sign frequently. We use magnetic field configuration with zero net magnetic

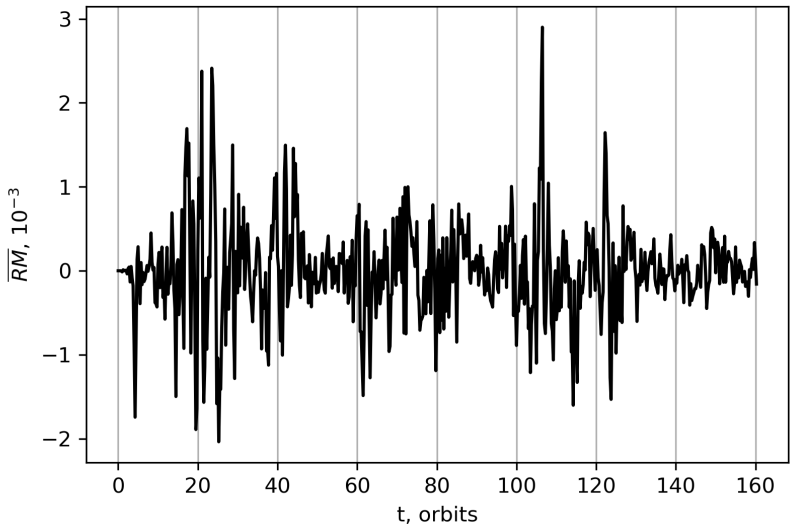


Figure 9 Time evolution of the horizontally averaged RM for the model SB2. RM is measured in arbitrary units.

flux and horizontally averaged B_z is close to zero at any given height and time. The spatial distributions of density fluctuations and B_z accounts for the sign of $\overline{RM}$. Such oscillating structure of $\overline{RM}$ is typical for all models. Especially large peak of $\overline{RM}$ is observed for the model SB1-Z at $t = 100$ orbits. Dependence $\overline{RM}\,(t)$ for the model SB1-Z is shown in Appendix A.

The structure of the horizontally averaged density is shown in Figure 10. The main vertical structure of density does not change significantly in time. There are quasi-periodical structures observed at $|z| > 2H$. Those uplifting motions are associated with the breakups of channel flows (Io and Suzuki 2014; Suzuki and Inutsuka 2009).

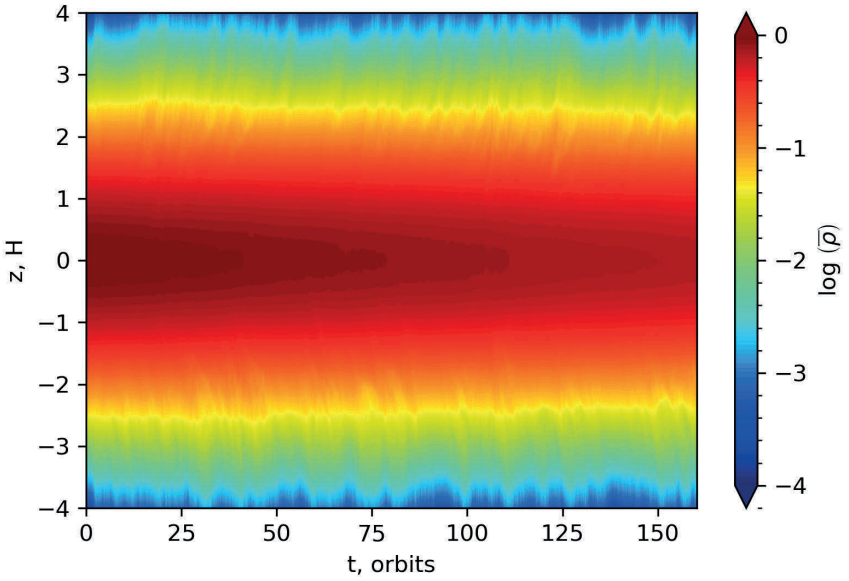


Figure 10 Time evolution of the horizontally averaged density ρ for the model SB2. Density ρ is measured in arbitrary units.

For investigation of correlations between RM and characteristics of turbulence and mass outflow we take an absolute value of RM and we also calculate moving averages of quantities under consideration ($|\overline{RM}|$, α and F_{bound}). For this purpose weighted moving averages are calculated using triangle filter with different numbers of data points N_{av} used for averaging. Then the pairwise cross-correlation functions between $|\overline{RM}|$, α and F_{bound} are calculated using the data sets obtained by averaging of data with variable number of N_{av}. The cross-correlation function between two data sets $X\,(t)$ and $Y\,(t)$ is defined as

$$R_{XY}\,(\tau) = \frac{\sum_t \left[(X\,(t) - \mu_X) \cdot (Y\,(t-\tau) - \mu_Y)\right]}{\sigma_X \cdot \sigma_Y}\,, \tag{11}$$

where μ_X and μ_Y are the mean values and σ_X and σ_Y are the standard deviations of respective data sets. Maximum value of cross-correlation function is used to characterize the level of correlations between the data sets. The duration of our calculations

is 160 orbits and our frequency of data acquisition is 4 files per orbit, so the total number of points in our data sets is $N = 640$.

3.3 Results of correlation analysis

Pairwise correlations are found between $|\overline{RM}|$, α and F_{bound} for all models. They were obtained in the following way. We start analysis of correlation functions with $N_{av} = 0$ that corresponds to the initial unsmoothed data and then we increase N_{av} parameter up to $N/2$. The maxima of cross-correlation functions increase with increasing N_{av} and they reach maximum value at $N_{av} \approx 51$. This value of N_{av} corresponds to the moving average taken over the interval of 12.5 orbits. Then the values of maxima of cross-correlation functions saturate and change little with the further increase of N_{av} and they drop when N_{av} becomes very large (comparable to half the number of data points $N/2$). The results described below correspond to the moving averages computed with $N_{av} = 51$.

The averaged characteristics $|\overline{RM}|$, α and F_{bound} for the fiducial model SB2 are shown in Appendix A. We obtain the following results for the model SB2: maxima of cross-correlation function between $|\overline{RM}|$ and α, between $|\overline{RM}|$ and F_{bound} and between α and F_{bound} are equal to 0.87, 0.69 and 0.76, correspondingly. The results of calculations of maxima of cross-correlation functions for all four models are shown in Table 2. There is no time delay, i.e. the maxima of cross-correlation functions described by Equation 11 are reached at $\tau = 0$. This holds for all results shown in Table 2. All pairwise correlations between three considered quantities are reasonably high for all our four models. There is no evident dependence of the results on grid resolution. These estimations provide quantitative confirmation that the properties of turbulence are connected with the properties of mass outflow and it is reflected in the structure of RM.

Table 2 Summary of the results of study of correlations between $|\overline{RM}|$, α and F_{bound} for four models.

Model	Maxima of cross-correlation functions between:		
	$\|\overline{RM}\|$ and α	$\|\overline{RM}\|$ and F_{bound}	α and F_{bound}
SB1	0.74	0.73	0.58
SB2	0.87	0.69	0.76
SB1-Z	0.92	0.6	0.63
SB2-Z	0.82	0.83	0.81

It is interesting to note that the time interval of data averaging that corresponds to maximal value of cross-correlation functions between the data sets (≈12 orbits) is close to a period of oscillations of the mean field B_y (≈10 orbits). It might be associated with vanishing of fast-oscillating chaotic turbulent fluctuations when applying moving averages with increasing N_{av} to the data. One could presume that the maximum of correlations corresponds to N_{av} associated with the main period of large time-scale turbulent oscillations and in our case it is approximately equal to the period of butterfly oscillations of B_y. However, as it was mentioned above, the maxima of

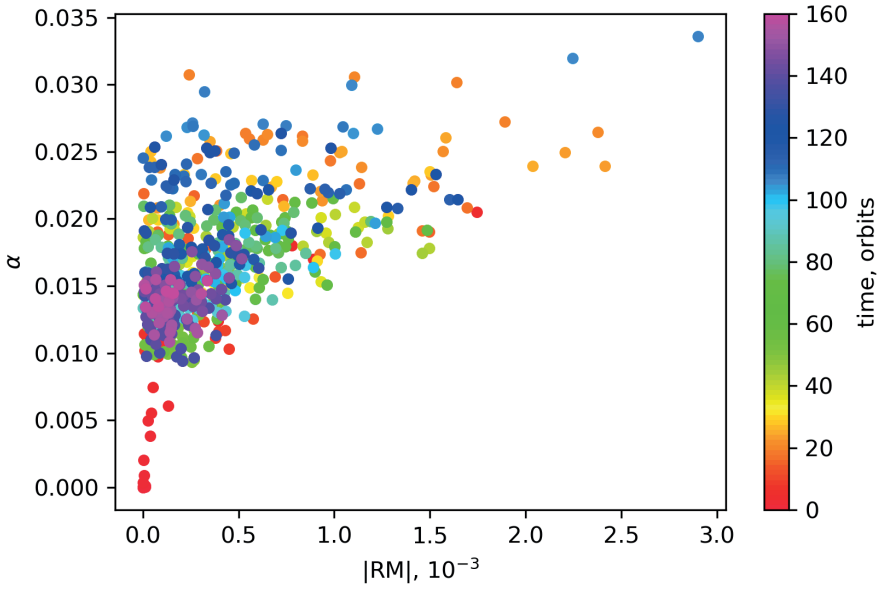


Figure 11 Dependence of α on $|\overline{RM}|$ for the model SB2. Initial unaveraged data are shown. Time evolution of α and $|\overline{RM}|$ is shown by colormap. RM is measured in arbitrary units.

correlations saturate with the further increase of N_{av}, so there is some ambiguity in estimations of the optimal value of N_{av}.

In Figures 11 and 12 we show dependence of α on $|\overline{RM}|$. Dependence of α on $|\overline{RM}|$ plotted for the initial unaveraged data is shown in Figure 11. There is no dependence between parameters and data points are scattered in conical area. It can be seen that the interval of values of $|\overline{RM}|$ is decreasing in time, e.g. in the time interval (40–100) orbits $|\overline{RM}|$ has values in the interval $(0–3)\cdot10^{-3}$ and in the time interval (100–160) orbits $|\overline{RM}|$ has values in the interval $(0–1.7)\cdot10^{-3}$. Dependence of α on $|\overline{RM}|$ plotted for averaged data is shown in Figure 12. From the start of the calculation until ≈ 40 orbits α and $|\overline{RM}|$ increase and reach their maximum values. The dependence between α and $|\overline{RM}|$ in the time interval (10–40) orbits can be well approximated by linear dependence. Then the parameters fluctuate around their mean values in the time interval (40–100) orbits, $\tilde{\alpha} = 0.016$ and $\widetilde{|\overline{RM}|} = 3.6\cdot10^{-4}$ and the dependence between them is also approximately linear. Both parameters reach local maxima at ≈ 110 orbits and then α continues to fluctuate around $\tilde{\alpha} = 0.016$ while the mean value of $|\overline{RM}|$ decreases to $2.8 \cdot 10^{-4}$ in the time interval (110–160) orbits. This decrease can be explained by the mass losses from the disk. At $t = 100$ orbits about 20% of the total mass of gas is lost and this decrease of gas density leads to the decrease of average $|\overline{RM}|$. As the mass of gas is lost from the computational domain with approximately constant rate, the average value of $|\overline{RM}|$ continuously decreases.

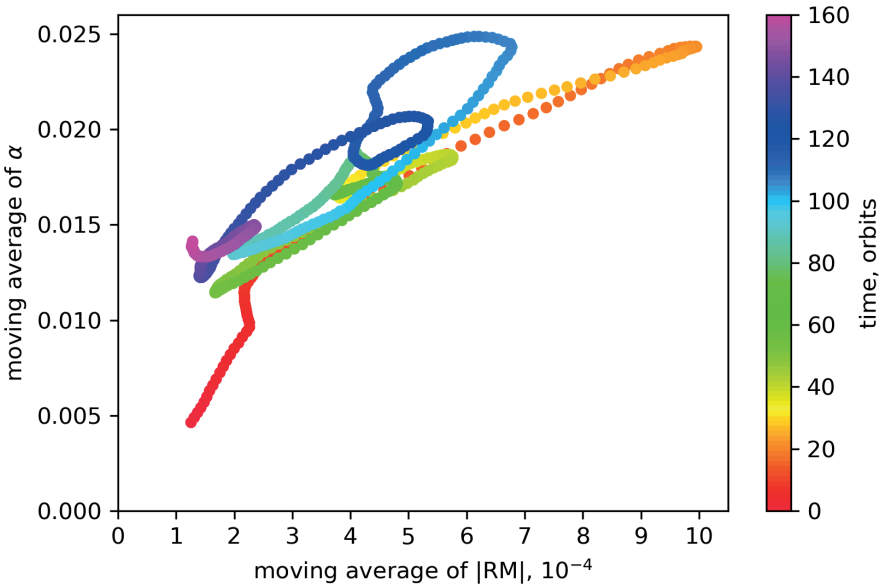


Figure 12 Dependence of α on $|\overline{RM}|$ for the model SB2. Averaged data are shown. Time evolution of α and $|\overline{RM}|$ is shown by colormap. RM is measured in arbitrary units.

3.4 Estimations of rotation measure in physical units

We use magnetic field configuration with zero net vertical magnetic flux in our calculations and it means that B_z has alternating-sign structure and B_z averaged over the fixed horizontal plane equals to zero. Therefore, the values of $\overline{RM}$ can be relatively small, e.g. the mean value of moving average of $|\overline{RM}|$ ($\sim 4 \cdot 10^{-4}$) normalized with mean values of density and field amplitude (~ 0.2 and ~ 0.1, correspondingly) is about $\dfrac{4 \cdot 10^{-4}}{0.2 \cdot 0.1} = 0.02$. It is of interest to estimate the values of $\overline{RM}$ in physical units and examine whether they can be observed in experiments.

It can be roughly estimated in the following way. The values of $\overline{RM}$ in our models can be compared with models with net vertical magnetic flux (such modeling is planned in the future work). One can roughly evaluate the magnitude of $\overline{RM}$ in case of uniform B_z assuming that the magnitude of constant B_z is equal to the amplitude of B_z oscillations in our model and the distribution of density ρ is similar to that in our case of B_z with zero net magnetic flux. The density cannot be significantly higher in the case of uniform B_z compared to our case because there is a mass flux through the vertical boundaries. With these assumptions, estimations using our density distributions show that $\overline{RM}$ is at most three orders of magnitude higher in the case of uniform B_z compared to the case of zero net magnetic flux. Measurements of RM in real sources, e.g. Sgr A* or M87* show that $RM \sim 10^5$ in jet. According to Park 2019, radial RM profile can be described as $RM \sim r^{-1}$, so RM in the disk is expected to be larger than RM in the jet. We can use the observed value of RM ($\sim 10^5$ rad/m^2) as a minimal RM value in the real disk. It means that RM in the case of zero net magnetic flux can be estimated as $RM > 10^2$ and is observable, e.g.

measurements of $\overline{RM} \sim 10^2$ rad/m^2 of polarized sources with VLA National Radio Astronomy Observatory are presented in the paper by Taylor et al. 2009.

Another method of estimating $\overline{RM}$ in physical units is to directly convert code units to physical units. The simulations are based on ideal MHD equations and they are scale invariant. There are three fundamental units in PLUTO code, which are length, density and velocity. Constants L_0, ρ_0, υ_0 are specified and they are used for units conversion: $\rho = \frac{\rho_{CGS}}{\rho_0}$, $L = \frac{L_{CGS}}{L_0}$, $\upsilon = \frac{\upsilon_{CGS}}{\upsilon_0}$, where variables with "CGS" subscript correspond to physical units, variables without subscript correspond to code units. For example, we can define fundamental constants for Sgr A* source as follows. We choose L_0 equals to Schwarzschild radius r_g, $L_0 = 1.25 \cdot 10^{12}$ cm; $\upsilon_0 = 5.5 \cdot 10^7$ cm/s corresponds to the characteristic sound speed in the disk (Falcke and Markoff 2013); $\rho_0 = B_{ref}^2/\upsilon_0^2$, where $B_{ref} = 1$ G is a characteristic magnetic field strength in the disk, in our case $\rho_0 = 3.31 \cdot 10^{-16}$ cm^{-3}. The unit of magnetic filed strength in PLUTO code is $B_0 = \sqrt{4\pi\rho_0\upsilon_0^2} = 3.54$ G. The standard formula for RM calculation is $RM[\text{rad/m}^2] = 8.1 \cdot 10^5 \int \rho[\text{cm}^{-3}] \cdot \text{B}_{\text{parallel}}[\text{G}] \cdot \text{ds}[\text{pc}]$, where B_{parallel} is the component of the magnetic field along the direction of the line of sight, integral is taken along the line of sight from the source to the observer (Carvalho and Ter Haar 1977). Using this formula we can obtain $\overline{RM}$ unit as $\overline{RM}_0[\text{rad/m}^2] = 8.1 \cdot 10^5 \rho_0[\text{cm}^{-3}] \cdot \text{B}_0[\text{G}] \cdot \text{L}_0[\text{pc}] = 6.5 \cdot 10^7$ rad/m^2. $\overline{RM}$ in the simulations can be estimated as $(10^{-4} - 10^{-3}) \cdot \overline{RM}_0 \sim (10^3 - 10^4)$ rad/m^2 and such values of $\overline{RM}$ are observable (Taylor et al. 2009).

In this way $\overline{RM}$ in physical units is roughly in the interval (10^2–10^4) rad/m^2 and it can be observed in experiments. More detailed discussion of applicability of the results to observations can be found below in Section 4.2.

4 Discussion

4.1 Physical meaning of correlations

RM, α and F_{bound} analysed in our models show oscillatory behaviour with fast turbulent oscillations with periods $< T$ and slow oscillations with periods about $10 \cdot T$. It is shown that the slow oscillations of these three quantities are correlated, i.e. their minima and maxima are reached approximately at the same time. The correlation levels are found to be in the interval ≈(0.60–0.90). Correlation levels for the pair of quantities $|\overline{RM}|$ and α are especially high and they lie in the interval (0.70–0.90). It means that measurements of RM can provide information about structure and periods of oscillations of α and F_{bound}, e.g. times of local maxima of RM approximately correspond to times of significant magnetic energy and mass flux outbursts and periods of RM oscillations are approximately equal to those of α and F_{bound}. Such correlations show that there is possible interconnection between $|\overline{RM}|$, α and F_{bound}, i.e. properties of F_{bound} and α can be studied by analysing the evolution of RM. However, additional work is needed to determine the exact physical origin of these correlations. Correlations may indicate the presence of some mechanism or process that causes periodic outbursts of magnetic energy and vertical mass flux. This process might be a dynamo process in disk since it leads to quasi-periodic oscillations of B_y with a

period approximately equal to the period of slow RM oscillations. Numerical experiments with shearing box models with different periods of the dynamo cycle could clarify whether the equality of periods of slow RM oscillations and dynamo cycle has physical meaning or it is a coincidence. Models with net magnetic flux need to be considered for such calculations, because the period of the dynamo-cycle is fixed in models with zero net vertical magnetic flux and it depends on initial magnetic field strength in models with net vertical magnetic flux (Bai and Stone 2013). This work is currently in progress.

4.2 Applications of results to observations

Velocities and mass outflow rates of disk winds can in principle be calculated using spectroscopy data (Balakrishnan et al. 2020). There are also theoretical and observational results that show a connection between the accretion rate and mass outflow rate in disks (e.g., Pudritz et al. 2007). The mass accretion rate can be estimated if the black hole mass and luminosity at some wavelength are known (Bian and Zhao 2003). So it may be possible to obtain an estimate of time evolution of vertical mass fluxes for black hole accretion disks in future observations. Such observations could provide information about correlation levels between $|\overline{RM}|$ and F_{bound} for real astrophysical disks. If one suggests that turbulence in real accretion disk can be described by the Shakura–Sunyaev model and the parameters of the disk correspond to those of considered disk models, the correlation levels between $|\overline{RM}|$ and F_{bound} are expected to be in an approximate interval of 0.50–0.95. The low level of correlations (≈ 0.1) between $|\overline{RM}|$ and F_{bound} in future observations may indicate that the real disk is incompatible with our model parameters and assumptions, e.g. it may indicate the presence of strong magnetic fields or absence of dynamo-effect in the source. In order to obtain estimates of correlation levels between $|\overline{RM}|$ and F_{bound} observations must have sufficient duration, which is at least 2 periods of RM oscillations, i.e. about 20 orbital periods.

The most likely candidates for future observations of accretion disks are sources Sgr A* and M87* (Event Horizon Telescope Collaboration 2021; Doeleman et al. 2019). Our calculations are non-relativistic. Measurements of RM and F_{bound} in real observations must be done at sufficiently large distance from the center of a black hole in order to avoid effects of general relativity. Such effects are present at the distance $r \approx 1 \cdot r_g$, where r_g is a gravitational radius. Value $100 \cdot r_g$ can be considered sufficiently large. If we suppose that observations of these sources are conducted at the radius $r = 100 \cdot r_g$, duration of observation of 20 orbital periods correspond to ≈ 85 days for Sgr A*. Such observations in principle could be conducted by the next-generation EHT (ngEHT) that will be operational before about 2030 (Doeleman et al. 2019). Imaging resolution of ngEHT is ≈ 10 μas (Chael et al. 2021), so the size of future images is about 20×20 pixels. One of the pixels can be monitored and RM data (evolution of RM) in this single pixel can be obtained. In this way the evolution of RM can be measured in future ngEHT observations. So correlation levels between RM and F_{bound} could be measured in real observations during the next decade.

4.3 Dependence on resolution and model parameters

The question of resolution dependence of the results in isothermal stratified shearing box simulations has not yet been solved. The study of convergence of the results with resolution for such simulations are contradictory. Some works report convergence of the results with resolution (e.g., Davis et al. 2010) while other research shows that the results do not converge (Bodo et al. 2014; Ryan et al. 2017).

Our lower resolution models have a resolution of 32 cells per scale height that marginally satisfies the condition of adequate MRI resolution. Our higher resolution models generally should provide more reliable results in description of physical processes than the lower resolution ones. But there is no qualitative difference between the results of correlation analysis for the models with lower and higher resolution. Additional study is done to investigate dependence of correlation levels on grid resolution on z axis. Correlational properties are studied for the models with resolutions on z axis equal to 256, 512 and 1024 grid zones per H (models with 1024 zones per H are not described in detail in this paper). The results of correlation analysis are found to be similar for all models. These results indicate that estimations of correlational properties of characteristics of the disk can be made using relatively low-resolution models with low computational cost. Additional calculations with higher resolution are required for further detailed study of dependence of results on grid resolution.

In this paper we study shearing box models with fixed initial magnetic field configuration and plasma β. However, in order to investigate properties and physical origin of correlations, presence and magnitude of correlations must be studied in models with other parameters (configurations of magnetic fields and plasma β). The results of additional calculations (which are not shown in this paper) with vertical (with zero net magnetic flux) and azimuthal magnetic field configurations and initial plasma β in range (10^0–10^3) show that correlations are present in all these models and there is no evident dependence of correlation levels on model parameters (Buldakov et al. 2022). Additional work on models with other magnetic field configuration and wider range of β is currently in progress.

4.4 Correlations in global disk

In this work we present results for shearing box models, which represent only a small part of accretion disk. It is of interest to investigate correlations between $|\overline{RM}|$, α and F_{bound} on larger spatial scales in global disk simulations. Such simulations also allow us to calculate the mass accretion rate $\dot{M}$ and study possible correlations between RM and $\dot{M}$. It is of interest because the mass accretion rate can be derived from observable quantities (Bechtold et al. 1987), so correlations between RM and $\dot{M}$ could be measured in observations. Such measurements could confirm or refute the results of the correlation analysis of model data.

5 Summary

In this paper we carried out calculations based on isothermal shearing box models. Our aim was to investigate possible interconnections between RM, α-parameter and total mass flux through vertical boundaries F_{bound}.

Our main conclusions were the following:

1. Simulations of shearing box using the Shakura–Sunyaev accretion disk model with zero net vertical magnetic flux predicted pairwise correlations between $|\overline{RM}|$, α and F_{bound} (illustration of correlations was shown in Figure 15). Correlations between $|\overline{RM}|$ and F_{bound} can be measured in future observations of Sgr A* by ngEHT. It means that compatibility of the model with real astrophysical disk can be tested in the next 10 years. Detection of such correlations in observations would confirm the validity of the standard stratified isothermal disk model with zero net vertical magnetic flux and this data could be used for further clarification of model details.

2. The periods of slow $|\overline{RM}|$, α and F_{bound} oscillations were found to be approximately equal to the period of the dynamo cycle. This finding in combination with pairwise correlations between $|\overline{RM}|$, α and F_{bound} showed the following:

   (a) Measurements of RM allow estimating periods of oscillations of α and F_{bound} and times of maxima and minima of these oscillations.

   (b) Measurements of RM allow estimating the period of the dynamo cycle.

   These conclusions are valid for the Shakura–Sunyaev accretion disk model with zero net vertical magnetic flux and $\beta_0 = 10^3$. These results also hold for additional calculations (which are not shown in this paper) with vertical and azimuthal magnetic field configurations and initial plasma β in range (10^0–10^3) (Buldakov et al. 2022). In order to experimentally obtain such estimations observations with duration of at least 20 orbital periods are needed and it corresponds to ≈ 85 days for Sgr A* provided that observations are conducted at the radius $r = 100 \cdot r_g$.

Acknowledgements

The authors would like to thank Evgenii Vasiliev for useful discussions, help with numerical modeling and helpful suggestions on preparation of the manuscript.

Appendix A Additional figures

In Figure 13 we show time and height dependence of the averaged azimuthal field $\overline{B_y}$ for the model SB1-Z.

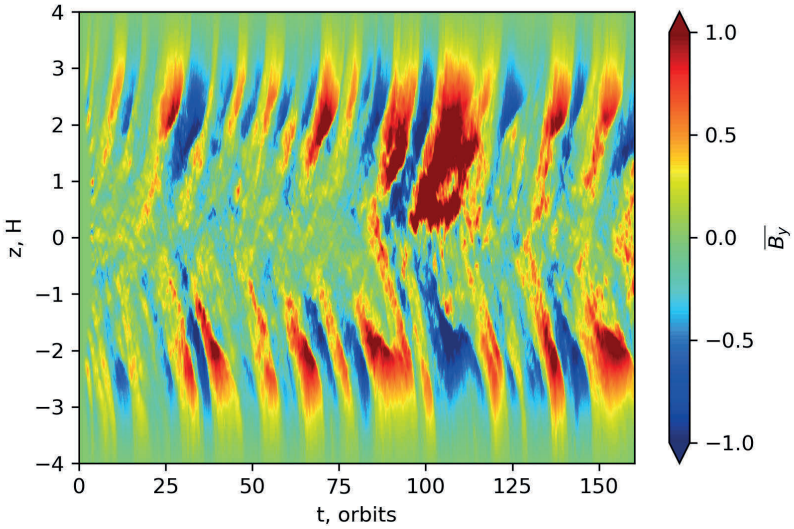


Figure 13 Contour plot of the horizontally averaged B_y for the model SB1-Z. B_y is measured in arbitrary units.

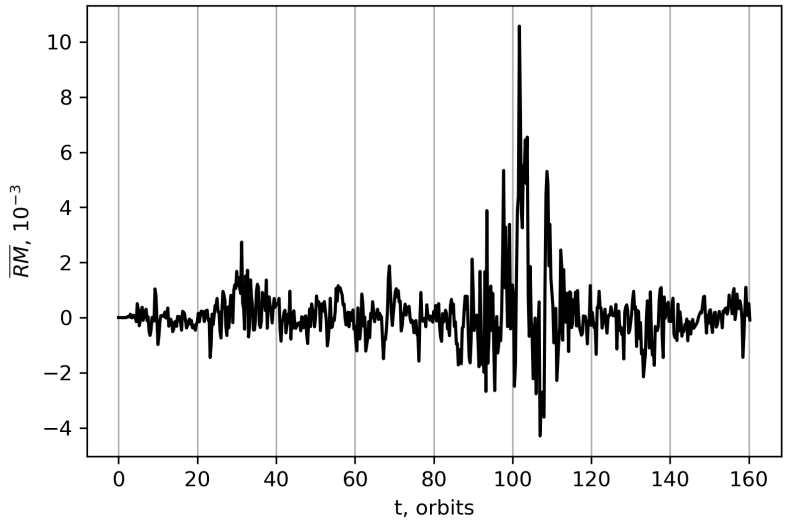


Figure 14 Time evolution of the horizontally averaged RM for the model SB1-Z. RM is measured in arbitrary units.

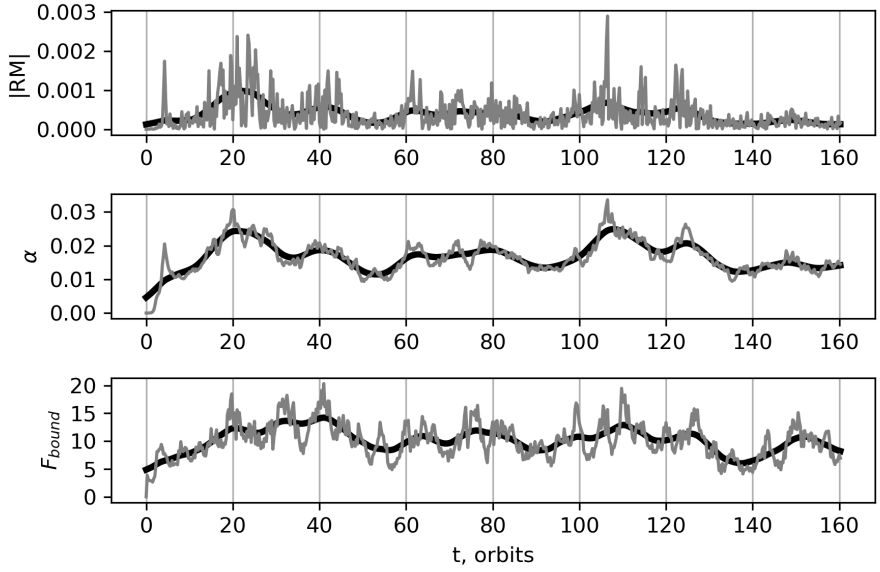


Figure 15 The averaged quantities $|\overline{RM}|$, α and F_{bound} for the model SB2 (black lines). Moving averages are calculated over the time interval of 12.5 orbits. Initial non-averaged data is shown for comparison with grey lines. $|\overline{RM}|$ and F_{bound} are measured in arbitrary units.

There are some irregularities in the duration and amplitude of the dynamo activity cycles and a particularly large outburst can be seen at $t = 105$ orbits. As it was mentioned above, such irregularities are observed for the models SB1 and SB1-Z with lower resolution, while models SB2 and SB2-Z with higher resolution have more regular and stable dynamo cycles.

In Figure 14 we show time evolution of $\overline{RM}$ for the model SB1-Z. A large peak can be observed at $t = 100$ orbits. This peak corresponds to the magnetic energy outburst shown above in Figure 13 and Figure 1.

In Figure 15 we present the averaged $|\overline{RM}|$, α and F_{bound} for the fiducial model SB2. All three averaged characteristics have similar structure, e.g. the major local maxima of characteristics are observed approximately at the same time. It indicates that the levels of pairwise correlations between them are expected to be relatively high.

References

Bai X.-N., Stone J.M. (2013) ApJ 767, 30
Balakrishnan M., Miller J.M., Trueba N. (2020) ApJ 893, 155
Balbus S.A., Hawley J.F. (1991) ApJ 376, 214
Balbus S.A., Hawley J.F. (1998) Reviews of Modern Physics 70, 1
Bechtold J., Czerny B., Elvis M. et al. (1987) ApJ 314, 699

Bian W.-H., Zhao Y.-H. (2003) PASJ 55, 599
Bodo G., Cattaneo F., Mignone A., Rossi P. (2014) ApJ 787, L13
Bower G.C., Wright M.C.H., Falcke H., Backer D.C. (2003) ApJ 588, 331
Brandenburg A., Nordlund A., Stein R.F., Torkelsson U. (1995) ApJ 446, 741
Brandenburg A. (2014) ApJ 791, 12
Buldakov M.A., Vasiliev E.O., Andrianov A.S. (2022) Astronomy at the Epoch of Multimessenger Studies, Proceedings of the BAK-2021 conference, held 23-28 August, 2021 in Moscow 274
Carvalho J.C., Ter Haar D. (1977) Ap&SS 51, 385
Chael A., Johnson M.D., Lupsasca A. (2021) ApJ 918, id. 6
Chandrasekhar S. (1960) Proceedings of the National Academy of Science 46, 253
Davis S.W., Stone J.M., Pessah M.E. (2010) ApJ 713, 52
Dhang P., Sharma P. (2019) MNRAS 482, 848
Doeleman S., Blackburn L., Dexter J. et al. (2019) in: Bulletin of the American Astronomical Society 51, 256
Event Horizon Telescope Collaboration, Akiyama K., Algaba J.C., Alberdi A. et al. (2021) ApJL 910, L12
Falcke H., Markoff S.B. (2013) Classical and Quantum Gravity 30, 244003
Flock M., Dzyurkevich N., Klahr H. et al. (2011) ApJ 735, 122
Fromang S., Latter H., Lesur G., Ogilvie G.I. (2013) A&A 552, A71
Gressel O. (2010) MNRAS 405, 41
Gressel O., Pessah M.E. (2015) ApJ 810, 59
Hawley J.F., Balbus S.A. (1991) ApJ 376, 223
Hawley J.F., Gammie C.F., Balbus S.A. (1995) ApJ 440, 742
Hawley J.F., Richers S.A., Guan X., Krolik J.H. (2013) ApJ 772, 102
Held L.E., Mamatsashvili G., Pessah M.E. (2024) MNRAS 530, 2232
Io Y., Suzuki T.K. (2014) ApJ 780, 46
Jiang Y.-F., Stone J.M., Davis S.W. (2013) ApJ 767, 148
Kuo C.Y., Asada K., Rao R. et al. (2014) ApJ 783, L33
Li Y.-P., Yuan F., Xie F.-G. (2016) ApJ 830, 78
Latter H.N., Fromang S., Gressel O. (2010) MNRAS 406, 848
Lesur G., Longaretti P.Y. (2007) MNRAS 378, 1471
Lynden-Bell D., Pringle J.E. (1974) MNRAS 168, 603
Marrone D.P., Moran J.M., Zhao J.-H., Rao R. (2007) ApJ 654, L57
Mignone A., Bodo G., Massaglia S. et al. (2007) ApJS 170, 228
Minoshima T., Hirose S., Sano T. (2015) ApJ 808, 54
Moll R. (2012) A&A 548, A76
Pudritz R.E., Ouyed R., Fendt C., Brandenburg A. (2007) in: Protostars and Planets V, eds. B. Reipurth, D. Jewitt and K. Keil, University of Arizona Press, Tucson, p. 277
Park J., Hada K., Kino M. et al. (2019) ApJ 871, article id. 257
Ryan B.R., Gammie C.F., Fromang S., Kestener P. (2017) ApJ 840, id. 6
Sano T., Inutsuka S.-i., Turner N.J., Stone J.M. (2004) ApJ 605, 321
Shakura N.I., Sunyaev R.A. (1973) A&A 24, 337
Sharma P., Quataert E., Stone J.M. (2007) ApJ 671, 1696
Shi J., Krolik J.H., Hirose S. (2010) ApJ 708, 1716
Stone J.M., Hawley J.F., Gammie C.F., Balbus S.A. (1996) ApJ 463, 656

Suzuki T.K., Inutsuka S.-i. (2009) ApJ 691, L49
Suzuki T.K., Muto T., Inutsuka S.-i. (2010) ApJ 718, 1289
Taylor A.R., Stil J.M., Sunstrum C. (2009) ApJ 702, 1230
Velikhov E.P. (1959) Journal of Experimental and Theoretical Physics 9, 995